Layered Insulator/Molecule/Metal Heterostructures with Molecular Functionality through Porphyrin Intercalation

Jacob Ducke[1,3], Alexander Riss[1,3], Alejandro Pérez Paz[2,3], Knud Seufert[1], Martin Schwarz[1], Manuela Garnica[1] , Angel Rubio[2,4,5], Willi Auwärter[1*]*

[1]Physik-Department E20, Technical University of Munich, James-Franck-Str.1, D-85748 Garching, Germany

[2]Nano-Bio Spectroscopy Group and ETSF, Universidad del País Vasco, 20018 San Sebastián, Spain

[3]School of Chemical Sciences and Engineering and School of Physical Sciences and Nanotechnology, Yachay Tech University, Urcuquí 100119, Ecuador

[4]Max Planck Institute for the Structure and Dynamics of Matter, Luruper Chaussee 149, 22761 Hamburg, Germany

[5]Center for Free-Electron Laser Science & Department of Physics, University of Hamburg, Luruper Chaussee 149, 22761 Hamburg, Germany

ABSTRACT

Intercalation of molecules into layered materials is actively researched in materials science (for the synthesis of van der Waals heterostructures), in chemistry (as a way to create nanoreactors), as well as in nanotechnology (to improve the technological applicability of surface-supported functional materials, which can be impaired by gaseous or liquid environment). However, the intercalation of organic molecules that exhibit physical or chemical functionality remains a key challenge to date. In this work we present the synthesis of heterostructures consisting of porphines sandwiched between a Cu(111) substrate and an insulating hexagonal boron nitride (*h*-BN) monolayer. We investigated the energetics of the intercalation, as well as the influence of the capping *h*-BN layer on the behavior of the intercalated molecules using scanning probe microscopy and density functional theory (DFT) calculations. While the self-assembly of the molecules is altered upon intercalation, we show that the intrinsic functionalities – such as switching between different porphine tautomers - are preserved. Such insulator/molecule/metal structures provide opportunities to protect organic materials from deleterious effects of atmospheric environment, can be used to control chemical reactions through geometric confinement, and give access to layered materials based on the ample availability of synthesis protocols provided by organic chemistry.

KEYWORDS: hexagonal boron nitride, intercalation, tautomerization, porphyrins, STM, nc-AFM, DFT

A promising approach for the fabrication of materials with tailored physical and chemical properties is the synthesis of hybrid materials by combination of different material classes (such as two-dimensional layers and organic molecular materials) at the nanoscale.[1–3] *h*-BN is

one of the prominent building blocks for such architectures due to its insulating behavior, high thermal conductivity, chemical and thermal stability.[1,4–6] Intercalation of atoms and small molecules has been studied for *h*-BN monolayers[7,8] and other two-dimensional materials such as graphene,[9,10] as well as for multilayer materials,[11,12] as a way to modify the materials' properties and to fabricate heterostructures that are not accessible *via* conventional delamination and transfer processes of two-dimensional materials.[13–20] Furthermore, reactions of small intercalated molecules (such as CO and ethylene) have been reported.[21–23] To date, only very few studies exist that can image intercalated molecular entities, such as C_{60} underneath graphene.[17,19,20] However, none of these studies investigate the intercalation of functional molecules and its impact on the intrinsic properties of intercalated molecules. For such purposes, porphyrins are a particularly interesting class of organic molecules, which have attracted much attention due to their widespread occurrence in biological systems and their potential application for solar energy harvesting and organic electronics.[24,25] The physicochemical behavior of porphyrins can be tuned *via* modification of their cores (with metal or hydrogen atoms) or their programmable substituents.[26]

Here we show the fabrication of layered architectures through the intercalation of molecules, demonstrated for unsubstituted porphyrins, *i.e.* porphines, at the *h*-BN/Cu(111) interface. We investigated the effect of the *h*-BN layer on the collective (*i.e.* self-assembly) and intrinsic (*i.e.* tautomerization) properties of the intercalated porphines in real space with sub-molecular resolution. The system was characterized using scanning probe microscopy: while non-contact atomic force microscopy (nc-AFM) yields detailed structural information on the capping *h*-BN layer, scanning tunneling microscopy (STM) allows imaging and manipulating the intercalated molecules due to the electronic transparency[27] of the *h*-BN layer. We found that the presence of the capping *h*-BN layer leads to the formation of a close-packed assembly of the intercalated molecules. Furthermore, we show that the intrinsic functionality

of hydrogen tautomerization of the porphines is preserved upon intercalation: reversible conductance switching can be triggered electronically *via* the STM tip. Density functional theory (DFT) calculations elucidate the energetics and the driving forces of the intercalation process. As intercalation and self-assembly of intercalated molecules can be triggered at relatively low temperatures, this synthesis procedure is a promising route for large scale bottom-up fabrication of protected functional nano-architectures and provides alternative synthesis protocols towards vertically stacked layered materials.

RESULTS AND DISCUSSION

Scanning probe measurements of intercalated porphines

The deposition of free-base porphines (2H-P, left structure in Fig. 1a) onto an *h*-BN-covered Cu(111) sample[27] held at 470 K leads to molecular assemblies with different appearances (Fig. 1a-c). In the vicinity of triangular-shaped holes[29] in the *h*-BN layer (marked by red arrows in Fig. 1b; such holes expose porphine-covered Cu(111)[30]) molecular assemblies with apparent heights of 0.04 nm (highlighted in yellow in Fig. 1b; V_s = 0.56 V) are observed. These molecules are intercalated, *i.e.* situated between the Cu(111) surface and the *h*-BN layer, as will be shown below. Additionally, brighter molecular units are found in Fig. 1b with apparent heights of 0.09 nm corresponding to 2H-Ps adsorbed on top of *h*-BN.[28] These molecules typically occupy positions close to defects, such as wrinkles in the *h*-BN layer.

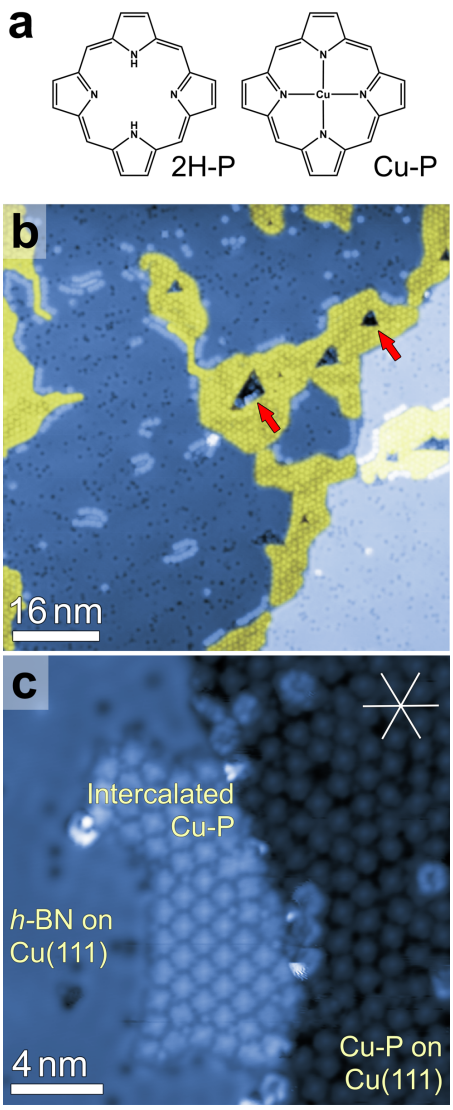

Figure 1. STM measurements of intercalated porphines at the *h*-BN/Cu(111) interface. The samples were prepared by deposition of free-base porphine (2H-P) onto *h*-BN/Cu(111) at 470 K. (a) Structural models of free-base porphine (2H-P) and copper porphine (Cu-P). (b) STM image with high coverage of *h*-BN shows pristine *h*-BN/Cu(111) regions, intercalated molecules (highlighted in yellow) in vicinity of triangular openings (marked with red arrows) in the h-BN layer providing doors for intercalation, as well as molecules adsorbed on *h*-BN (V_s = 0.56 V, I = 77 pA). (c) STM image of sample with *h*-BN grown at submonolayer-coverage shows three regions: (i) *h*-BN/Cu(111), (ii) intercalated self-assembled porphines that underwent self-metalation with Cu adatoms, and (iii) self-metalated porphines on Cu(111). Lines in the top right indicate the dense-packed high symmetry directions of the Cu(111) substrate (V_s = 0.34 V, I = 330 pA).

For samples with lower *h*-BN coverage, *i.e.* with larger exposed Cu(111) areas, three different regions were observed (Fig. 1c, V_s = 0.34 V): (i) A region with pristine *h*-BN on Cu(111) (labeled "*h*-BN on Cu(111)"). (ii) A region where the exposed Cu(111) surface is covered with molecules (labeled "Cu-P on Cu(111)"), which exhibit an irregular arrangement with average neighbor distances of 1.27 ± 0.05 nm. The molecules miss the typical depression observed in free-base species,[30] instead they show a bright protrusion in their centers indicative of metalated copper porphines (Cu-P, Fig. 1a) (self-metalation of porphyrins typically takes place at temperatures below the annealing temperature of 470 K used here[31–33]). Additionally, individual porphines adsorbed in the second molecular layer, *i.e.* on top of the Cu-P, are imaged as bright species in this region. (iii) A region where the molecular units self-assemble into a two-dimensional lattice (labeled "Intercalated Cu-P" in Fig. 1c and highlighted in yellow in Fig. 1b) with a nearest neighbor (NN)-distance of 1.11 ± 0.05 nm. Analysis of the STM data reveals a superstructure matrix of $\begin{pmatrix} 5 & 3 \\ 2 & -3 \end{pmatrix}$ for intercalated Cu-Ps with respect to the underlying Cu(111) substrate. The direction of one porphine axis along opposite N atoms in the macrocycle is closely aligned with a dense-packed high symmetry direction of the Cu(111) surface (see structure model below). The molecules in this region show substantially lower corrugations (0.03 nm) compared to the Cu-Ps on bare Cu(111) (0.08 nm) and 2H-Ps on *h*-BN/Cu(111) (0.09 nm).

Combined STM/nc-AFM measurements give direct evidence that the self-assembled porphine arrays (Fig. 1) are intercalated between Cu(111) and *h*-BN. The STM image in Fig. 2a (V_s = 1 V, I = 15 pA) shows an *h*-BN/Cu-P/Cu(111) region (top left) and an *h*-BN/Cu(111) region (bottom right). The molecules are imaged as circular features exhibiting ordered packing. Four Cu-P centers (*i.e.* local height maxima) are marked with yellow dots in Fig. 2a, their equivalent positions (taking into account sample drift) are plotted also in Fig. 2b-d. The

nc-AFM measurement in Fig. 2b displays the frequency shift (Δf) at constant tip height of the same area showing atomic resolution of the *h*-BN layer on top of Cu-P/Cu(111) (lattice constant of $a_{h\text{-BN}}$ = 0.25 nm[27,34]) confirming that the molecules are situated underneath the *h*-BN layer.

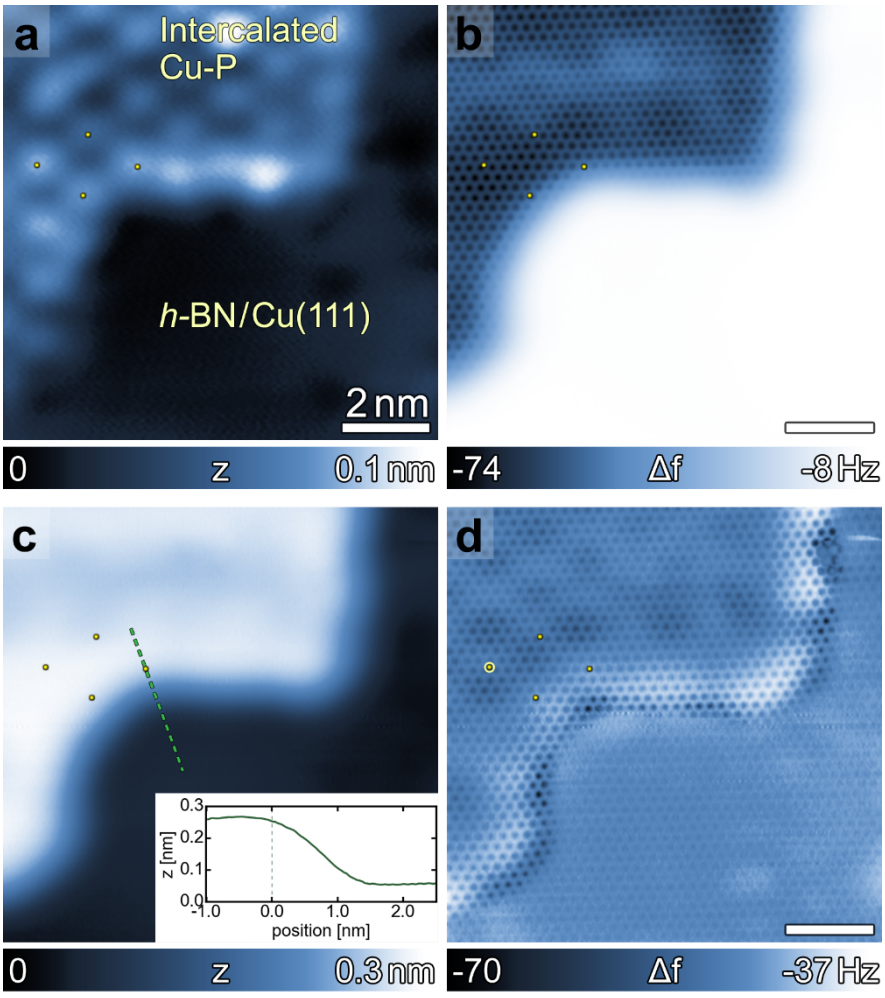

Figure 2. High-resolution STM/nc-AFM measurements of intercalated molecules. (a) *h*-BN/Cu-P/Cu(111) imaged in constant-current STM mode (V_s = 1 V, I = 15 pA) shows ordered arrangement of intercalated molecules (yellow dots mark positions of four Cu-P centers). The flat region in the bottom right shows pristine *h*-BN/Cu(111). (b) Constant-height AFM measurement (V_s = 0 V) of the same area shows atomic resolution of the h-BN lattice on top of the *h*-BN/Cu-P/ Cu(111). (c) Constant-Δf measurement (V_s = 0 V, Δf = -20 Hz) shows an apparent height difference of $\Delta h_{h\text{-BN}}$= 0.21 nm between the *h*-BN/Cu-P/Cu(111) and *h*-BN/Cu(111). Height profile along the dashed line is shown in inset (position x = 0 nm

is defined as the center of the Cu-P highlighted with a yellow dot). (d) Two-pass AFM measurement (height offset of -0.090 nm with respect to (c)) shows atomically resolved *h*-BN lattice across both regions. The yellow circle marks the uncertainty of the positions of the molecular centers due to sample drift.

A slight variation of the frequency shift (~4 Hz) at the length scale of nanometers can be observed. Due to the significantly higher tip-sample distance in the *h*-BN/Cu(111) region the frequency shift is higher (imaged brighter due to lower attractive forces) and shows no pronounced atomic-scale contrast. To investigate the change of the *h*-BN height due to the intercalation, we conducted a constant-Δf AFM experiment (*i.e.* a feedback loop adjusts z to keep the frequency shift set point of Δf = -20 Hz), which is shown in Fig. 2c. The applied voltage was set to V_s = 0 V (see section S2 in the Supporting Information for voltage dependent measurements). In the inset of Fig. 2c a height profile along the dashed line in Fig. 2c is depicted. Measurements on different islands yield an average height difference of $\Delta h_{h\text{-}BN}$ = 0.21 ± 0.02 nm between *h*-BN/Cu-P/Cu(111) and *h*-BN/Cu(111). Atomic resolution over the whole *h*-BN layer can be achieved in a two-pass AFM experiment[35] (Fig. 2d). Here the tip follows the height profile of Fig. 2c with an additional height offset of Δz = -0.090 nm (z-feedback is switched off) and Δf is recorded. This way, the *h*-BN lattice can be resolved across the whole range of the image (see section S3 in the Supporting Information for a discussion of the varying contrast). Thus, this combination of nc-AFM and STM measurements gives direct evidence for the intercalation of molecules below a continuous *h*-BN sheet.

Electronic structure of Co-Porphines

We performed dI/dV spectroscopy to investigate the influence of the adsorption position on the electronic structure of the molecules. For these experiments we used cobalt porphines

(Co-Ps), because the resonances associated with the Co atoms in the dI/dV spectra contain information about the electronic coupling of the molecules to the metal support.[36] The Co-Ps were deposited and intercalated following the same procedure described above for the 2H-Ps. The inset in Fig. 3 shows an STM image with Co-Ps on top of the *h*-BN (linearly arranged) and an island of intercalated molecules (on the right side). The spectrum of Co-P on *h*-BN/Cu(111) (grey dotted trace) exhibits a pronounced peak at V_s = 1.1 V, which is attributed to Co states,[33,37] as well as a resonance at V_s = -2.2 V, which is attributed to the porphine HOMO (the energy can vary depending on the position of the molecule on the Moiré structure[28]). The relatively sharp peaks, as well as the negative differential resistance (NDR) at sample biases V_s > 1.3 V, are indicative of an efficient electronic decoupling of the molecules from the metal surface.[36] The spectrum for Co-P on Cu(111) (red dashed trace) shows an increase of the local density of states for higher positive biases (V_s > 0.7 V), but no sharp features in the investigated voltage range. This is likely caused by broadening due to electronic coupling with the metal surface.[38] Similarly, the spectrum of the intercalated Co-P (blue solid trace) exhibits only very broad features indicating electronic interaction with the metallic support.

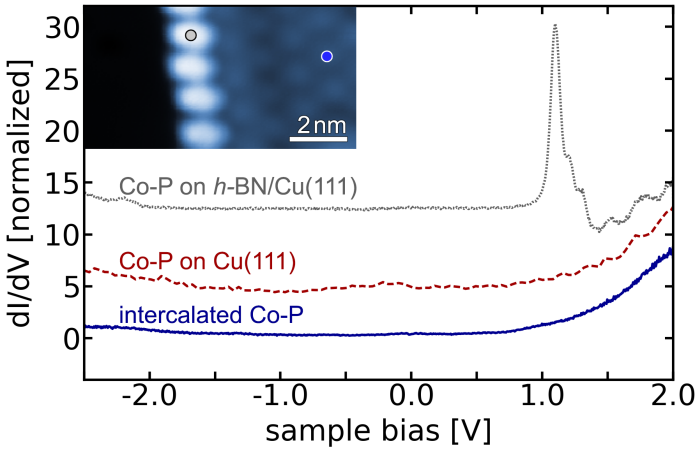

Figure 3. dI/dV spectroscopy of Co-Ps in different environments. Spectrum of Co-P on *h*-BN/Cu(111) (grey dotted trace) exhibits characteristic peak attributed to Co states.[33,37]

Spectrum of Co-P on Cu(111) (red dashed trace) shows no sharp features arising from molecular resonances. Similarly, spectrum of intercalated Co-P (blue solid trace) also shows only very broad features. The spectra are normalized by their respective values at V_s = -2.2 V and vertically offset for clarity. Inset shows STM image with spectroscopy positions for Co-P on *h*-BN (grey dot) and intercalated Co-P (blue dot) – the tip was positioned above the molecular centers in all cases.

Switching of intercalated free-base porphines

As dI/dV spectroscopy indicates that the electronic structure of the porphines on Cu(111) is not significantly altered by the capping *h*-BN layer, the next step was to investigate electronically induced tautomerization reactions.[39-41] As outlined above, elevated temperatures that promote the intercalation process also lead to self-metalation of the molecules. Thus, in most of our experiments Cu-Ps are the predominant species. However, by reducing the time for which the sample temperature is above the metalation temperature, some 2H-Ps can be preserved and identified in STM scans of the intercalated islands. The dashed black circle in Fig. 4a-c marks such an intercalated 2H-P with its characteristic twofold symmetry and a depression in the center (in contrast to the neighboring spherically symmetric Cu-Ps with bright centers).[33] Application of a voltage pulse (V_s = 1.6 V, t = 15 s, I = 2-5 nA) with the STM tip positioned close to the center of the intercalated molecule induces an apparent rotation of the intramolecular features by 90 degrees (compare Fig. 4a and b) indicating a transformation to the other trans tautomer of 2H-P. A second voltage pulse with the same parameters can be used to restore the original symmetry orientation (Fig. 4c). A typical current vs. time trace with the tip held at constant height above the intercalated molecule shows switching between two distinct conductance levels (Fig. 4h). Simulations of the STM images for the two trans tautomers of the 2H-P on Cu(111) (Fig. 4e and g) resemble the experimental images that were obtained in the switching experiments (Fig. 4a-c). Both tautomers exhibit two-fold symmetry, but in experiment as well as in theory one of the

tautomers (Fig. 4a,c,e) exhibits brighter features along the N-H bond direction. This is likely caused by a different alignment of the amino hydrogen atoms with respect to the Cu surface: while the tautomer in Fig. 4d has the two amino N-H bonds aligned along the short bridge sites of the Cu(111) surface,[42] the amino bonds of the other tautomer (Fig. 4f) are aligned along the long bridge sites, with the H atoms adsorbed on the hollow sites (the most stable adsorption mode of 2H-P on Cu(111)). According to our DFT calculations, both 2H-P tautomers are nearly isoenergetic with a small energy difference of 0.1 eV. Switching between the two forms is triggered by tunneling induced vibrational excitations of the molecule[40,41] and corresponds to a change of the positions of the central amino hydrogen atoms. A 90-degree rotation of the whole 2H-P could in principle yield similar results, however such a rotation is unlikely as neighboring molecules inhibit the rotation (see also section S8 in the Supporting Information). Furthermore, we have not observed tip-induced lateral movement of the intercalated molecules suggesting a high barrier for translation and rotation of the intercalated molecules. An (additional) change of the adsorption configuration of the 2H-P cannot be ruled out entirely, but the symmetry of the molecular appearance in STM (Fig. 4a-c) and the presence of two distinct conductance states (Fig. 4h) suggests that tunneling-facilitated hydrogen tautomerization takes place.[43,44] We thus conclude that the intrinsic functionality of porphine switching is preserved upon intercalation, *i.e.* underneath a capping monolayer of *h*-BN.

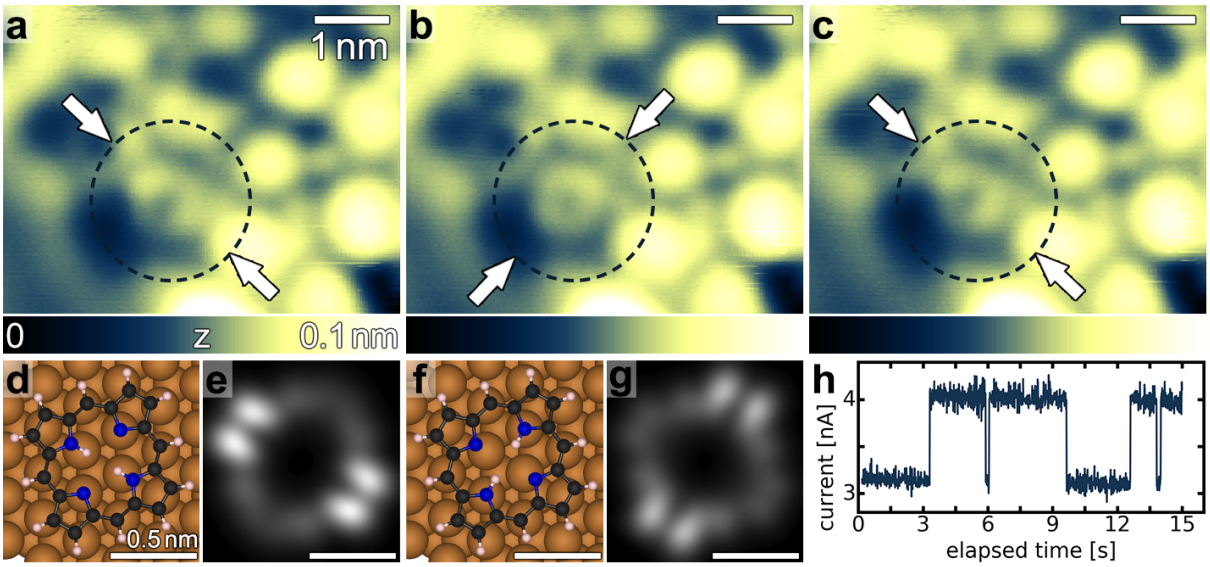

Figure 4. Proton tautomerization of an intercalated free-base porphine. (a) The twofold symmetry of the intercalated 2H-P (dashed black circle) can be resolved in STM measurements (V_s = 0.5 V, I = 200 pA for (a)-(c)). (b) STM image of the same area as in (a) reveals the other trans tautomer after application of a voltage pulse of 1.6 V. (c) Another voltage pulse with the same parameters reverts the 2H-P configuration back to its initial state as seen in (a). White arrows in (a)-(c) indicate the orientation of the pyrrolic hydrogens. (d),(f) DFT-optimized structures of the two possible trans tautomers of 2H-P adsorbed on Cu(111) (Cu: brown, N: blue, C: black, H: white). (e), (g) STM simulations (V_s = 0.5 V) for the two tautomers. (h) Current *vs*. time trace recorded with the tip positioned above the molecule marked by the dashed black circle in (a)-(c) reveals switching between two distinct conductance levels (V_s = 1.6 V, t = 15 s).

Energetics of the intercalation process

The mechanism of the intercalation involves delamination of the of *h*-BN starting at the edges of the weakly bonded layer from the Cu(111) substrate,[45] such that intercalated islands can be formed through molecular diffusion. Thus the intercalated molecular islands (consisting of 2H-P, Cu-P or Co-P) are observed close to edges, as well as holes in the *h*-BN layer which are commonly found at domain boundaries (these holes are large enough such that porphines

can adsorb on the exposed surface). No clear preference for intercalation at one of these defect types was found (see Fig. S5 in the Supporting Information).

The sizes of most of the intercalated islands are significantly smaller than 100 nm^2, which hints at a diffusion-limited process (as opposed to edge-delamination being the limiting step[10]). It is possible that the intercalation process is in some cases assisted by pre- or co-intercalation of small atomic or molecular species that can diffuse underneath the *h*-BN without inducing substantial geometric distortions[15] (see Fig. S1 in the Supporting Information). The activation energy associated with the delamination of the *h*-BN layer is reflected in the onset temperature of the intercalation process of about 420 K. Furthermore, our measurements show that efficient porphine intercalation occurs only at temperatures below 470 K, which can be explained by facile desorption of molecules at elevated temperatures.

To investigate the energetics and driving forces of the intercalation process in detail, we performed DFT calculations including long-range van der Waals (*vdW*) interactions.[46] The optimized geometries for the three experimentally observed adsorption arrangements are shown in Fig. 5 along with their corresponding calculated adsorption energies ΔE: (a) Cu-P on Cu(111) with ΔE_1 = -4.63 eV, (b) 2H-P on *h*-BN/Cu(111) with ΔE_2 = -2.58 eV, (c) intercalated Cu-P with ΔE_3 = -1.18 eV. The adsorption energies were calculated with respect to the separate constituents, consisting of an isolated porphine and the *h*-BN/Cu(111) or the Cu(111) surface, respectively:

$$\Delta E_1 = E(Cu\text{-}P/Cu(111)) - \left[E(Cu\text{-}P) + E\big(Cu(111)\big)\right]$$

$$\Delta E_2 = E(2H\text{-}P/h\text{-}BN/Cu(111)) - \left[E(2H\text{-}P) + E\big(h\text{-}BN/Cu(111)\big)\right]$$

$$\Delta E_3 = E(h\text{-}BN/Cu\text{-}P/Cu(111)) - \left[E(Cu\text{-}P) + E\big(h\text{-}BN/Cu(111)\big)\right]$$

where E(x) are the calculated energies of the relaxed geometries of structure x. Please note that the metalation energy is not included in these calculations, *i.e.* we assume that for the

formation of intercalated Cu-Ps metalation precedes the intercalation. This is in line with temperature-dependent experiments indicating that the activation energy for metalation is lower than the activation energy for intercalation (see also section S6 in the Supporting Information for a discussion of the metalation energy).

The intercalation is driven by the large adsorption energy of the molecules on the Cu(111), ΔE_1 = -4.63 eV, however, as the *vdW* interaction between *h*-BN and Cu(111) weakens when Cu-P intercalates, a smaller intercalation energy gain of ΔE_3 = -1.18 eV results. In the calculations we used a 5x5x4 slab comprising 4 layers of copper atoms (25 atoms per layer), a total of 25 B and 25 N atoms in the *h*-BN layer, and one porphine. In this small supercell, the *h*-BN structure is rather flat. The separation between neighboring Cu-Ps is 1.28 nm, which is close to the experimentally observed (NN)-distance of a = 1.11 ± 0.05 nm for intercalated molecules. In calculations, the vertical separation between *h*-BN and the top layer of Cu(111) without intercalated molecules, $h_{h\text{-BN/Cu(111)}}$ = 0.315 nm, agrees quite well with Refs.[27,45,47,48]. Upon intercalation the calculated vertical distance between *h*-BN and the top layer of Cu(111) increases to $h_{h\text{-BN/Cu-P/Cu(111)}}$ = 0.566 nm. Therefore, the difference between these two heights is $\Delta h_{h\text{-BN}}$ = 0.251 nm. This is slightly larger than the height difference that was determined from nc-AFM experiments averaged over different molecular islands ($\Delta h_{h\text{-BN}}$ = 0.21 ± 0.02 nm). This difference can be caused by a variation in the long-range forces (such as electrostatic forces) on top of *h*-BN/Cu(111) and *h*-BN/Cu-P/Cu(111) – this also explains the reduced atomic contrast on top of the *h*-BN/Cu(111) areas in Fig. 2d (a larger tip-sample distance in this area leads to a reduced contrast). The adsorption height with respect to the molecular center of mass for the intercalated Cu-P was calculated to be h = 0.230 nm compared to h = 0.235 nm for Cu-P on Cu(111). Both systems show significant charge transfer from the metal surface to the molecule: 1.45 e^- for the intercalated Cu-P and 1.29 e^- for the Cu-P on Cu(111), as calculated by DFT. The *h*-BN plays almost no role in the charge

transfer but causes the vertical separation between porphine molecule and Cu(111) topmost layer to be slightly reduced (~0.05 nm). In contrast, for the 2H-P on *h*-BN/Cu(111) only a very small charge transfer of 0.06 e^- is predicted (at an adsorption height of 0.334 nm above *h*-BN).

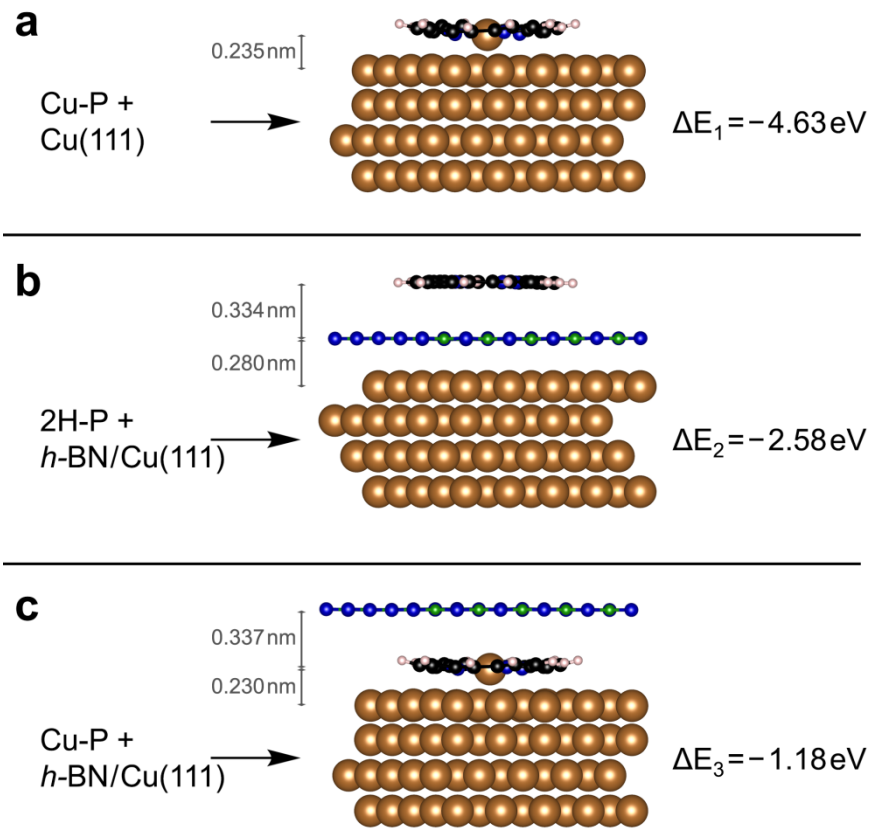

Figure 5. DFT-optimized structures and respective energies for the experimentally observed porphine arrangements: (a) Cu-P on Cu(111) with ΔE_1 = -4.63 eV, (b) 2H-P on *h*-BN/Cu(111) with ΔE_2 = -2.58 eV, and (c) intercalated Cu-P with ΔE_3 = -1.18 eV. The side views of calculated structures for 5x5x4 Cu(111) slabs are shown (Cu: brown, N: blue, B: green, C: black, H: white). Calculated vertical heights of porphine center of mass with respect to the average of the Cu(111) top layer (or the *h*-BN layer, respectively) are given.

It is important to note that all three adsorption processes (Fig. 5) are thermodynamically favorable. This is in agreement with our experiments, in which we observe all three adsorption arrangements. Based on the calculated adsorption energies, the simulations predict

that the porphines preferably adsorb on Cu(111), followed by *h*-BN/Cu(111) and the intercalated molecules. The intercalated Cu-Ps are therefore predicted to exist in the smallest quantity. In fact, we observe in the experiments that intercalation only takes place when the exposed Cu(111) surface is completely covered by molecules. However, we typically observe a higher abundance of intercalated molecules compared to the number of molecules adsorbed on *h*-BN/Cu(111). For instance, Fig. 1b shows that only very few molecules are adsorbed on *h*-BN/Cu(111) (most of which are located close to defect sites, such as wrinkles in the *h*-BN). This discrepancy between experiment and theory can be explained by several factors: (i) Overbinding between *h*-BN and Cu(111) can occur in the theoretical modelling caused by the overestimation of C_6 coefficients in the *vdW* correction used,[45,49] which (ii) can be particularly relevant for the modelled *h*-BN/Cu(111) registry (N atoms on-top of Cu atoms) representing the strongest interaction within the Moiré lattice[27] (see also section S4 in the Supporting Information). (iii) Also, the influence of different surface diffusion barriers might play a role in the experiments (*i.e.* porphine migration is readily possible from *h*-BN/Cu(111) towards Cu(111), but not in the opposite direction). (iv) Furthermore, porphine desorption from h-BN – which occurs at elevated temperatures during sample preparation – is hindered for the intercalated molecules. (v) The calculations clearly show the effect of the density of the intercalated porphines on the energy gain ΔE_a: The reduction of the (NN)-distance from a = 2.05 nm (8x8x4 slab) to a = 1.28 nm (5x5x4 slab) results in the intercalation energy changing its sign from an thermodynamically unfavorable situation with +4.8 eV to a favorable case with -1.18 eV. Higher densities (or smaller unit cells) thus yield a higher energy gain as the decrease of *vdW* interaction energy between *h*-BN and Cu(111) is smaller per intercalated molecule. According to this trend the energy gain due to intercalation will further increase for the experimentally observed (NN)-distance of 1.11 ± 0.05 nm and thus explain the higher

prevalence of intercalated species observed in experiment. This coverage effect is also likely the cause for the dense self-assembly of the intercalated molecules.

CONCLUSIONS

In conclusion, we have synthesized hybrid inorganic-organic heterostructures consisting of porphine molecules (2H-P, Cu-P or Co-P) intercalated between Cu(111) and an *h*-BN layer at moderate temperatures. The intercalation process is driven by the high adsorption energy of the molecules on the metal surface and the formation of new *vdW* contacts between the porphines and *h*-BN; in a closed-packed molecular assembly this energy gain can compensate the energy cost for delamination of *h*-BN (*i.e.* reduction of *vdW* interaction between *h*-BN and Cu(111)). The capping *h*-BN layer does not significantly alter the electronic properties of the molecules: tautomerization can be triggered by injecting electrons through the *h*-BN layer. This work opens up potential pathways towards the use of functional molecular architectures outside of ultrahigh vacuum environments. Furthermore, chemical reactions of intercalated molecules[21,50] could be controlled by geometric confinement and the selectivity of the intercalation process to different reactants.

METHODS

All experiments were performed in custom-designed ultrahigh-vacuum chambers housing a commercial STM/nc-AFM operated at T = 5 K (CreaTec). The base pressure during the experiments was below $2 \cdot 10^{-10}$ mbar. Repeated cycles of Argon sputtering and annealing to 725 K were used to prepare the Cu(111) single crystal. h-BN was grown from the precursor borazine at a pressure of $7 \cdot 10^{-7}$ mbar and a sample temperature of 1070 K.[27] Subsequently, 2H-P molecules (Sigma Aldrich, purity ≥99%) were evaporated from a thoroughly degassed quartz crucible held at 470 K. During deposition the sample temperature was kept at 420 –

470 K. All STM images were recorded in constant-current mode using an electrochemically etched tungsten tip. nc-AFM measurements were performed using a qPlus sensor with a tungsten tip (resonance frequency ~25 kHz, oscillation amplitude 80 pm, Q value ~ 79000). dI/dV spectra were acquired at constant height (open feedback loop) with a lock-in amplifier using a modulation frequency of 470 Hz – 770 Hz and a modulation voltage of 14 mV – 35 mV (r.m.s.). Current traces I(t) were recorded at constant height (open feedback loop).

Slab calculations were performed using the projector augmented wave pseudo-potential method[51] as implemented in the VASP code.[52-55] We used the PBE exchange-correlation functional in all calculations.[56] We included long-range *vdW* interactions *via* the Tkatchenko-Scheffler approach.[46] The convergence threshold of the electronic cycle was set to 10^{-5} eV. The Cu(111) surface was modeled with the coordinates derived from a typical PBE lattice constant of 0.363 nm.[42,48] The low (high) coverage limit was modeled *via* 8x8x4 (5x5x4) slabs that feature lateral porphine separations of 2.053 (1.283) nm. The adsorption mode of 2H-P on Cu(111) of Müller *et al*.,[42] which places the two N-H amino (=N- imino) groups of 2H-P along the long (short) bridge position, agrees well with our experimental observations and was adopted for all porphine molecules on Cu(111). The B-N distance in *h*-BN (0.1482 nm) was stretched slightly (< 3 %) with respect to its experimental value (0.1446 nm) so as to achieve commensurate unit cells with the underlying Cu(111) surface.[57] The adsorption of h-BN on Cu(111) is dominated by *vdW* interactions and we use a model that places the N atoms on-top Cu atoms and B over fcc sites.[27,47,48] The optimal adsorption site of a single Cu adatom on the Cu(111) surface is the 3-fold fcc site according to STM experiments and DFT calculations.[58] The *h*-BN, adsorbate, adatoms, and the top Cu layer were relaxed until all ionic forces were below 2.5 eV/nm. These geometry optimizations used a kinetic energy cutoff of 400 eV and 3x3x1 (1x1x1) k-point sampling for 5x5x4 (8x8x4) slabs. For accurate energetics, single point energy calculations were performed at a 600 eV cutoff and 5x5x1

(3x3x1) k-point grid for 5x5x4 (8x8x4) slabs. Over 1.8 nm of vacuum and dipole corrections were used to decouple the periodic images along the normal z direction. We used spin polarized calculations whenever necessary (Cu-P species). The charge transfers were computed *via* the Bader analysis code.[59] STM images were simulated under the Tersoff-Hamann approximation.[60]

ASSIOCIATED CONTENT

The authors declare no competing financial interest.

Supporting Information

The Supporting Information is available free or charge on the ACS Publications website.

Additional AFM, STM, and DFT data.

AUTHOR INFORMATION

Corresponding Authors

*Alexander Riss, E-mail: a.riss@tum.de

*Willi Auwärter, E-mail: wau@tum.de

Author Contributions

‡ These authors contributed equally to this work. W.A. conceived the experiments. J.D. and A.Ri. performed the STM/nc-AFM measurements and analyzed the data. A.P.P. performed the theoretical calculations. K.S. and M.S. helped with the experiments. W.A. supervised the experiments and helped with the interpretation. A.Ru. supervised the theoretical calculations

and helped with the interpretation. J.D. and A.Ri. wrote the manuscript with help from A.P.P. and W.A.. All authors discussed the results and helped with the manuscript.

ACKNOWLEDGMENTS

This work was financially supported by the European Research Council Consolidator Grant NanoSurfs (no. 615233). We acknowledge financial support from the European Research Council (ERC-2015-AdG-694097), Grupos Consolidados (IT578-13), and European Union's H2020 programme under GA no.676580 (NOMAD) and GA no. 646259 (MOSTOPHOS). W.A. acknowledges funding by the DFG *via* a Heisenberg professorship. A.P.P. acknowledges postdoctoral fellowship from the Spanish "Juan de la Cierva-incorporación" program (IJCI-2014-20147). We want to thank Jascha Repp and Franz J. Gießibl for support regarding the instrumental setup.

REFERENCES

(1) Geim, A. K.; Grigorieva, I. V. Van Der Waals Heterostructures. *Nature* **2013**, *499*, 419–425.

(2) Liu, Y.; Weiss, N. O.; Duan, X.; Cheng, H.-C.; Huang, Y.; Duan, X. Van Der Waals Heterostructures and Devices. *Nat. Rev. Mater.* **2016**, *1*, 16042.

(3) Sanchez, C.; Shea, K. J.; Kitagawa, S. Recent Progress in Hybrid Materials Science. *Chem. Soc. Rev.* **2011**, *40*, 471–472.

(4) Widmer, R.; Berner, S.; Gröning, O.; Brugger, T.; Osterwalder, J.; Greber, T. Electrolytic *In Situ* STM Investigation of h-BN-Nanomesh. *Electrochem. Commun.* **2007**, *9*, 2484–2488.

(5) Haigh, S. J.; Gholinia, A.; Jalil, R.; Romani, S.; Britnell, L.; Elias, D. C.; Novoselov, K. S.; Ponomarenko, L. A.; Geim, A. K.; Gorbachev, R. Cross-Sectional Imaging of Individual Layers and Buried Interfaces of Graphene-Based Heterostructures and superlattices. *Nat. Mater.* **2012**, *11*, 764–767.

(6) Pakdel, A.; Bando, Y.; Golberg, D. Nano Boron Nitride Flatland. *Chem. Soc. Rev.* **2014**, *43*, 934–959.

(7) Mertens, S. F. L.; Hemmi, A.; Muff, S.; Gröning, O.; Feyter, S. de; Osterwalder, J.; Greber, T. Switching Stiction and Adhesion of a Liquid on a Solid. *Nature* **2016**, *534*, 676–679.

(8) Fedorov, A.; Praveen, C. S.; Verbitskiy, N. I.; Haberer, D.; Usachov, D.; Vyalikh, D. V.; Nefedov, A.; Wöll, C.; Petaccia, L.; Piccinin, S.; Sachdev, H.; Knupfer, M.; Büchner, B.; Fabris, S.; Grüneis, A. Efficient Gating of Epitaxial Boron Nitride Monolayers by Substrate Functionalization. *Phys. Rev. B* **2015**, *92*, 125440.

(9) Al Balushi, Zakaria Y.; Wang, K.; Ghosh, R. K.; Vilá, R. A.; Eichfeld, S. M.; Caldwell, J. D.; Qin, X.; Lin, Y.-C.; DeSario, P. A.; Stone, G.; Subramanian, S.; Paul, D. F.; Wallace, R. M.; Datta, S.; Redwing, J. M.; Robinson, J. A. Two-Dimensional Gallium Nitride Realized *via* Graphene Encapsulation. *Nat. Mater.* **2016**, *15*, 1166–1171.

(10) Grånäs, E.; Knudsen, J.; Schröder, U. A.; Gerber, T.; Busse, C.; Arman, M. A.; Schulte, K.; Andersen, J. N.; Michely, T. Oxygen Intercalation under Graphene on Ir(111): Energetics, Kinetics, and the Role of Graphene Edges. *ACS Nano* **2012**, *6*, 9951–9963.

(11) Kovtyukhova, N. I.; Wang, Y.; Lv, R.; Terrones, M.; Crespi, V. H.; Mallouk, T. E. Reversible Intercalation of Hexagonal Boron Nitride with Brønsted Acids. *J. Am. Chem. Soc.* **2013**, *135*, 8372–8381.

(12) Smith, R. P.; Weller, T. E.; Howard, C. A.; Dean, M. P.; Rahnejat, K. C.; Saxena, S. S.; Ellerby, M. Superconductivity in Graphite Intercalation Compounds. *Physica C: Superconductivity and its Applications* **2015**, *514*, 50–58.

(13) Ma, C.; Park, J.; Liu, L.; Kim, Y.-S.; Yoon, M.; Baddorf, A. P.; Gu, G.; Li, A.-P. Interplay Between Intercalated Oxygen Superstructures and Monolayer h -BN on Cu(100). *Phys. Rev. B* **2016**, *94*, 64106.

(14) Martínez-Galera, A. J.; Schröder, U. A.; Huttmann, F.; Jolie, W.; Craes, F.; Busse, C.; Caciuc, V.; Atodiresei, N.; Blügel, S.; Michely, T. Oxygen Orders Differently under Graphene: New Superstructures on Ir(111). *Nanoscale* **2016**, *8*, 1932–1943.

(15) Petrović, M.; Šrut Rakić, I.; Runte, S.; Busse, C.; Sadowski, J. T.; Lazić, P.; Pletikosić, I.; Pan, Z.-H.; Milun, M.; Pervan, P.; Atodiresei, N.; Brako, R.; Šokčević, D.; Valla, T.; Michely, T.; Kralj, M. The Mechanism of Caesium Intercalation of Graphene. *Nat. Commun.* **2013**, *4*, 2772.

(16) Usachov, D.; Adamchuk, V. K.; Haberer, D.; Grüneis, A.; Sachdev, H.; Preobrajenski, A. B.; Laubschat, C.; Vyalikh, D. V. Quasifreestanding Single-Layer Hexagonal Boron Nitride as a Substrate for Graphene Synthesis. *Phys. Rev. B* **2010**, *82*, 75415.

(17) Monazami, E.; Bignardi, L.; Rudolf, P.; Reinke, P. Strain Lattice Imprinting in Graphene by C 60 Intercalation at the Graphene/Cu Interface. *Nano Lett.* **2015**, *15*, 7421–7430.

(18) Ohtomo, M.; Sekine, Y.; Wang, S.; Hibino, H.; Yamamoto, H. Etchant-Free Graphene Transfer Using Facile Intercalation of Alkanethiol Self-Assembled Molecules at graphene/metal interfaces. *Nanoscale* **2016**, *8*, 11503–11510.

(19) Varykhalov, A.; Gudat, W.; Rader, O. Imaging Buried Molecules: Fullerenes under Graphene. *Adv. Mater.* **2010**, *22*, 3307–3310.

(20) Lu, J.; Zheng, Y.; Sorkin, A.; Loh, K. P. Growing Suspended Graphene on C 60 Molecules. *Small* **2012**, *8*, 3728–3732.

(21) Fu, Q.; Bao, X. Surface Chemistry and Catalysis Confined under Two-Dimensional Materials. *Chem. Soc. Rev.* **2017**, 1842–1874.

(22) Zhang, Y.; Weng, X.; Li, H.; Li, H.; Wei, M.; Xiao, J.; Liu, Z.; Chen, M.; Fu, Q.; Bao, X. Hexagonal Boron Nitride Cover on Pt(111): A New Route to Tune Molecule–Metal Interaction and Metal-Catalyzed Reactions. *Nano Lett.* **2015**, *15*, 3616–3623.

(23) Yang, Y.; Fu, Q.; Li, H.; Wei, M.; Xiao, J.; Wei, W.; Bao, X. Creating a Nanospace under an h-BN Cover for Adlayer Growth on Nickel(111). *ACS Nano* **2015**, *9*, 11589–11598.

(24) Yella, A.; Lee, H.-W.; Tsao, H. N.; Yi, C.; Chandiran, A. K.; Nazeeruddin, M. K.; Diau, E. W.-G.; Yeh, C.-Y.; Zakeeruddin, S. M.; Gratzel, M. Porphyrin-Sensitized Solar Cells with Cobalt (II/III)-Based Redox Electrolyte Exceed 12 Percent Efficiency. *Science* **2011**, *334*, 629–634.

(25) Lindsey, J. S.; Bocian, D. F. Molecules for Charge-Based Information Storage. *Acc. Chem. Res.* **2011**, *44*, 638–650.

(26) Auwärter, W.; Écija, D.; Klappenberger, F.; Barth, J. V. Porphyrins at Interfaces. *Nat. Chem.* **2015**, *7*, 105–120.

(27) Joshi, S.; Ecija, D.; Koitz, R.; Iannuzzi, M.; Seitsonen, A. P.; Hutter, J.; Sachdev, H.; Vijayaraghavan, S.; Bischoff, F.; Seufert, K.; Barth, J. V.; Auwärter, W. Boron Nitride on Cu(111): An Electronically Corrugated Monolayer. *Nano Lett*. **2012**, *12*, 5821–5828.

(28) Joshi, S.; Bischoff, F.; Koitz, R.; Ecija, D.; Seufert, K.; Seitsonen, A. P.; Hutter, J.; Diller, K.; Urgel, J. I.; Sachdev, H.; Barth, J. V.; Auwärter, W. Control of Molecular Organization and Energy Level Alignment by an Electronically Nanopatterned Boron Nitride Template. *ACS Nano* **2014**, *8*, 430–442.

(29) Lu, J.; Yeo, P. S. E.; Zheng, Y.; Xu, H.; Gan, C. K.; Sullivan, M. B.; Castro Neto, A. H.; Loh, K. P. Step Flow *Versus* Mosaic Film Growth in Hexagonal Boron Nitride. *J. Am. Chem. Soc*. **2013**, *135*, 2368–2373.

(30) Bischoff, F.; Seufert, K.; Auwärter, W.; Joshi, S.; Vijayaraghavan, S.; Écija, D.; Diller, K.; Papageorgiou, A. C.; Fischer, S.; Allegretti, F.; Duncan, D. A.; Klappenberger, F.; Blobner, F.; Han, R.; Barth, J. V. How Surface Bonding and Repulsive Interactions Cause Phase Transformations: Ordering of a Prototype Macrocyclic Compound on Ag(111). *ACS Nano* **2013**, *7*, 3139–3149.

(31) Diller, K.; Klappenberger, F.; Marschall, M.; Hermann, K.; Nefedov, A.; Wöll, C.; Barth, J. V. Self-Metalation of 2H-Tetraphenylporphyrin on Cu(111): An X-ray Spectroscopy Study. *J. Chem. Phys*. **2012**, *136*, 14705.

(32) Marbach, H. Surface-Mediated *in Situ* Metalation of Porphyrins at the Solid–Vacuum Interface. *Acc. Chem. Res*. **2015**, *48*, 2649–2658.

(33) Diller, K.; Papageorgiou, A. C.; Klappenberger, F.; Allegretti, F.; Barth, J. V.; Auwärter, W. In Vacuo Interfacial Tetrapyrrole Metallation. *Chem. Soc. Rev*. **2016**, *45*, 1629–1656.

(34) Paszkowicz, W.; Pelka, J. B.; Knapp, M.; Szyszko, T.; Podsiadlo, S. Lattice Parameters and Anisotropic Thermal Expansion of Hexagonal Boron Nitride in the 10-297.5 K Temperature Range. *Appl. Phys. A: Mater. Sci. Process.* **2002**, *75*, 431–435.

(35) Moreno, C.; Stetsovych, O.; Shimizu, T. K.; Custance, O. Imaging Three-Dimensional Surface Objects with Submolecular Resolution by Atomic Force Microscopy. *Nano Lett.* **2015**, *15*, 2257–2262.

(36) Tu, X. W.; Mikaelian, G.; Ho, W. Controlling Single-Molecule Negative Differential Resistance in a Double-Barrier Tunnel Junction. *Phys. Rev. Lett.* **2008**, *100*, 126807.

(37) Urgel, J. I.; Schwarz, M.; Garnica, M.; Stassen, D.; Bonifazi, D.; Ecija, D.; Barth, J. V.; Auwärter, W. Controlling Coordination Reactions and Assembly on a Cu(111) Supported Boron Nitride Monolayer. *J. Am. Chem. Soc.* **2015**, *137*, 2420–2423.

(38) Repp, J.; Meyer, G.; Stojković, S. M.; Gourdon, A.; Joachim, C. Molecules on Insulating Films: Scanning-Tunneling Microscopy Imaging of Individual Molecular Orbitals. *Phys. Rev. Lett.* **2005**, *94*, 26803.

(39) Liljeroth, P.; Repp, J.; Meyer, G. Current-Induced Hydrogen Tautomerization and Conductance Switching of Naphthalocyanine Molecules. *Science* **2007**, *317*, 1203–1206.

(40) Auwärter, W.; Seufert, K.; Bischoff, F.; Ecija, D.; Vijayaraghavan, S.; Joshi, S.; Klappenberger, F.; Samudrala, N.; Barth, J. V. A Surface-Anchored Molecular Four-Level Conductance Switch Based on Single Proton Transfer. *Nat. Nanotechnol.* **2011**, *7*, 41–46.

(41) Kumagai, T.; Hanke, F.; Gawinkowski, S.; Sharp, J.; Kotsis, K.; Waluk, J.; Persson, M.; Grill, L. Thermally and Vibrationally Induced Tautomerization of Single Porphycene Molecules on a Cu(110) Surface. *Phys. Rev. Lett.* **2013**, *111*, 246101.

(42) Müller, M.; Diller, K.; Maurer, R. J.; Reuter, K. Interfacial Charge Rearrangement and Intermolecular Interactions: Density-Functional Theory Study of Free-Base Porphine Adsorbed on Ag(111) and Cu(111). *J. Chem. Phys.* **2016**, *144*, 24701.

(43) Koch, M.; Pagan, M.; Persson, M.; Gawinkowski, S.; Waluk, J.; Kumagai, T. Direct Observation of Double Hydrogen Transfer *via* Quantum Tunneling in a Single Porphycene Molecule on a Ag(110) Surface. *J. Am. Chem. Soc.* **2017**, *139*, 12681–12687.

(44) Novko, D.; Blanco-Rey, M.; Tremblay, J. C. Intermode Coupling Drives the Irreversible Tautomerization in Porphycene on Copper(111) Induced by Scanning Tunnelling Microscopy. *J. Phys. Chem. Lett.* **2017**, *8*, 1053–1059.

(45) Schwarz, M.; Riss, A.; Garnica, M.; Ducke, J.; Deimel, P. S.; Duncan, D. A.; Thakur, P. K.; Lee, T.-L.; Seitsonen, A. P.; Barth, J. V.; Allegretti, F.; Auwärter, W. Corrugation in the Weakly Interacting Hexagonal-BN/Cu(111) System: Structure Determination by Combining Noncontact Atomic Force Microscopy and X-ray Standing Waves. *ACS Nano* **2017**, *11*, 9151–9161.

(46) Tkatchenko, A.; Scheffler, M. Accurate Molecular Van Der Waals Interactions from Ground-State Electron Density and Free-Atom Reference Data. *Phys. Rev. Lett.* **2009**, *102*, 73005.

(47) Gómez Díaz, J.; Ding, Y.; Koitz, R.; Seitsonen, A. P.; Iannuzzi, M.; Hutter, J. Hexagonal Boron Nitride on Transition Metal Surfaces. *Theor. Chem. Acc. (Theoretical Chemistry Accounts)* **2013**, *132*, 1350.

(48) Koitz, R.; Seitsonen, A. P.; Iannuzzi, M.; Hutter, J. Structural and Electronic Properties of a Large-Scale Moiré Pattern of Hexagonal Boron Nitride on Cu(111) Studied with Density Functional Theory. *Nanoscale* **2013**, *5*, 5589.

(49) Jensen, F. The Basis Set Convergence of Spin−Spin Coupling Constants Calculated by Density Functional Methods. *J. Chem. Theory Comput.* **2006**, *2*, 1360–1369.

(50) Petrosko, S. H.; Johnson, R.; White, H.; Mirkin, C. A. Nanoreactors: Small Spaces, Big Implications in Chemistry. *J. Am. Chem. Soc.* **2016**, *138*, 7443–7445.

(51) Blöchl, P. E. Projector Augmented-Wave Method. *Phys. Rev. B* **1994**, *50*, 17953–17979.

(52) Kresse, G.; Furthmüller, J. Efficient Iterative Schemes for *ab Initio* Total-Energy Calculations Using a Plane-Wave Basis Set. *Phys. Rev. B* **1996**, *54*, 11169–11186.

(53) Kresse, G.; Hafner, J. *Ab Initio* Molecular Dynamics for Liquid Metals. *Phys. Rev. B* **1993**, *47*, 558–561.

(54) Kresse, G.; Hafner, J. Norm-Conserving and Ultrasoft Pseudopotentials for First-Row and Transition Elements. *J. Phys.: Condens. Matter* **1994**, *6*, 8245–8257.

(55) Kresse, G.; Joubert, D. From Ultrasoft Pseudopotentials to the Projector Augmented-Wave Method. *Phys. Rev. B* **1999**, *59*, 1758–1775.

(56) Perdew, J. P.; Burke, K.; Ernzerhof, M. Generalized Gradient Approximation Made Simple. *Phys. Rev. Lett.* **1996**, *77*, 3865–3868.

(57) Nag, A.; Raidongia, K.; Hembram, K. P. S. S.; Datta, R.; Waghmare, U. V.; Rao, C. N. R. Graphene Analogues of BN: Novel Synthesis and Properties. *ACS Nano* **2010**, *4*, 1539–1544.

(58) Repp, J.; Meyer, G.; Rieder, K.-H.; Hyldgaard, P. Site Determination and Thermally Assisted Tunneling in Homogenous Nucleation. *Phys. Rev. Lett.* **2003**, *91*, 206102.

(59) Tang, W.; Sanville, E.; Henkelman, G. A Grid-Based Bader Analysis Algorithm Without Lattice Bias. *J. Phys.: Condens. Matter* **2009**, *21*, 84204.

(60) Tersoff, J.; Hamann, D. R. Theory of the Scanning Tunneling Microscope. *Phys. Rev. B* **1985**, *31*, 805–813.

TOC Graphic